Measurement report: Formation of tropospheric brown carbon in a lifting air mass

Can Wu[1,2], Xiaodi Liu[1], Ke Zhang[1], Si Zhang[1]*, Cong Cao[3,4], Jianjun Li[3], Rui Li[1,2], Fan Zhang[1,2], Gehui Wang[1,2]*

[1]Key Lab of Geographic Information Science of the Ministry of Education, School of Geographic Sciences, East China Normal University, Shanghai 210062, China
[2]Institute of Eco-Chongming, 20 Cuiniao Rd., Chongming, Shanghai 202150, China
[3]State Key Laboratory of Loess and Quaternary Geology, Institute of Earth Environment, Chinese Academy of Sciences, Xi'an 710061, China
[4]School of Marine and Atmospheric Science, Stony Brook University, Stony Brook, NY 11794, USA

*Corresponding authors: Dr. Si Zhang, E-mail: szhang@geo.ecnu.edu.cn
Prof. Gehui Wang, E-mail: ghwang@geo.ecnu.edu.cn

Abstract: An enhanced formation of brown carbon (BrC) with a non-negligible warming effect at the tropopause has recently been found. However, its formation mechanism is unclear. Here we report a BrC formation process that happens during air mass upward transport by conducting simultaneously a 4-hour time resolution of measurement on atmospheric BrC at the mountain foot (MF, 400m a.s.l.) and mountainside (MS, 1120m a.s.l.) of Mt. Hua, China in 2016 summer. Our results showed that the daytime light-absorption (Abs_{365nm}) of BrC at MS is approximately 60% lower than that at MF due to a dilution effect caused by the planetary boundary layer expansion, but the daytime light-absorption of BrC relative to black carbon at MS is about 30% higher than that at MF, suggesting a significant formation of secondary BrC in the lifting process of air mass from MF to MS. Such a secondary formation accounted for >50% of BrC at MS but only 27% of BrC at MF. Moreover, N:C elemental ratio of the daytime BrC was 15% higher at MS than that at MF, mainly due to an aerosol aqueous phase formation of water-soluble organic nitrogen (WSON) compounds. Stable nitrogen isotope composition further indicated that such light-absorbing WSON compounds were produced from the aerosol aqueous-phase reaction of carbonyls with NH_4^+. Our work for the first time revealed that ammonia -induced aerosol aqueous reactions can significantly promote BrC formation during the air mass lifting process, which is probably responsible for an enhanced light absorption of BrC in the upper boundary layer.

Keywords: Brown carbon; Ammonia and carbonyls; Nitrogen-containing organic compounds; Air mass upward transport; Aerosol aqueous-phase reaction.

1. Introduction

Light-absorbing organic aerosols, known as brown carbon (BrC), can efficiently absorb solar radiation in the visible to near ultraviolet (UV) wavelength range (Laskin et al., 2015; Liu et al., 2020a; Chakrabarty et al., 2023a) which is corresponding to 27~70% of black carbon (BC) light-absorption in the lower troposphere (Saleh et al., 2015; Lin et al., 2014; Lin et al., 2015) suggesting that BrC can perturb substantially the planetary radiation budget (Qian et al., 2015; Lin et al., 2014; Liu et al., 2015). By absorbing solar radiation at short wavelengths, BrC can strongly alter local gas-phase photochemistry and atmospheric oxidation through decreasing the photolysis rates of OH radicals, NO_2 and O_3, leading to a reduction in atmospheric oxidant concentration by up to ~30% (Hammer et al., 2016; Gligorovski et al., 2015; Jo et al., 2016). BrC in the atmosphere also acts as photosensitizers and produces active intermediates, and thus can promote sulfate formation (Liu et al., 2020b). In addition, BrC comprises numerous organic species and can induce adverse human health effects, because some of chromophores are toxic (Huang et al., 2018; Hsu et al., 2014; Yan et al., 2018).

Atmospheric BrC has both primary and secondary sources. Biomass burning is believed to be the major source of primary BrC (Chakrabarty et al., 2023b), while emissions from fossil fuel combustion is also an important source of primary BrC in the urban atmosphere (Yan et al., 2017; Corbin et al., 2019), which accounts for even more than 40% of the total BrC in heating season (Li et al., 2023). In the past decades numerous studies reported that BrC can also be secondarily generated in the atmosphere, such as photooxidation of aromatics under high NOx conditions (Lin et al., 2015; Liu et al., 2021), NH_4^+-initiated reactions with atmospherically relevant carbonyls (Li et al., 2021b; Kampf et al., 2012; Laskin et al., 2014; Li et al., 2019b)

and ·OH/NO_3· radical oxidations of various VOCs (Sumlin et al., 2017; Gelencser et al., 2003; Lu et al., 2011). BrC is chemically active, which may undergo photobleaching (Schnitzler et al., 2022; Gilardoni et al., 2016), posing significant challenges for characterizing BrC molecular composition and its links to optical properties.

Recently a aircraft measurement conduced over the continental United States observed an enhanced short-wavelength optical absorption of BrC relative to BC at altitudes between 5 and 12 km (Zhang et al., 2017), indicating that secondary formation is one of crucial sources for these high-altitude BrC. Numerical model studies reported that global radiative forcing caused by BrC ranges from 0.1-0.6 Wm^{-2} (Zhang et al., 2020; Lin et al., 2014; Druge et al., 2022), suggesting a non-negligible impact of BrC on the global climate change. Studies found that such climate effects are highly sensitive to BrC and the sensitivity rapidly increases along with an increase in altitude (Zhang et al., 2017; Nazarenko et al., 2017; Hodnebrog et al., 2014). These abundant BrC at the tropopause would bring about prominent impacts on radiative forcing, which is even twice of that induced by low-altitude BrC (Zhang et al., 2017). Due to the limited number of field observations, however, the vertical distribution and formation mechanism of tropospheric BrC are still unclear especially those in the upper troposphere, where the direct radiative forcing of BrC is much stronger than that in the ground surface atmosphere.

To elucidate the formation mechanism of BrC in the troposphere, synchronous observations on atmospheric BrC were conducted on the mountainside and the mountain foot of Mt. Hua, which is located closely to Guanzhong Basin, one of the areas with heaviest $PM_{2.5}$ pollution in China owing to intensive activities of fossil fuel combustion and the unfavorable

topography (Wang et al., 2022b; Wu et al., 2020; Wang et al., 2011; Wang et al., 2016). Our previous study has shown that inorganic aerosol chemistry in the atmosphere over Mt. Hua is dominated by the air mass transport from the Guanzhong Basin ground surface, in which $(NH_4)_2SO_4$ is continuously produced during the air mass lifting process along with a decrease in aerosol acidity (Wu et al., 2022). Here, we investigated the formation mechanism of secondary BrC during the lifting process of air mass from the Guanzhong Basin to the mountainous atmosphere of Mt. Hua. We firstly discussed the differences in vertical distribution and optical absorption of water-soluble BrC between the ground surface and the mountainous atmosphere, then explored their formation mechanism in the upper boundary layer. To the best of our knowledge, we for the first time found that ammonia-induced aerosol aqueous phase reaction with carbonyls is the dominant formation pathway of BrC in the air mass lifting process, which is responsible for the high ratio of BrC to BC in the top troposphere.

2. Materials and Methods

2.1 Sample Collection

Offline $PM_{2.5}$ samples with a 4-hour interval were synchronously collected onto prebaked quartz filters (at 450 ℃ for 6 h) at two locations of Mt. Hua from 27 August to 17 September 2016. One sampling site locates at the mountain foot (MF, 34°32′N, 110°5′E; 400 m a.s.l.) and another one is situated on the mountainside (MS; 34°29′N, 110°3′E; 1120 m a.s.l.) with little anthropogenic activities due to its steep terrain in the mountain region. The horizontal distance between the two sites is ~8 km and the vertical distance is about 1km (Figure S1). As revealed in our previous study (Wu et al., 2022), vertical divergence simulated by WRF-Chem model

decreased gradually as enhanced elevation, along with the prevailing southerly winds, indicating a feasibility of vertical transport of air parcel from MF to MS. And we also note that the change of emission sources among two site was insignificant in a lifting air mass as indicated by indistinctive divergences of diagnostic ratios and proportion of organic tracers from emission sources. Such conditions can avoid the interferences caused by the emission sources change when exploring aging process of BrC. More descriptions on the two sites have been documented by our previous study along with the details on the sampling instrument setup (Wu et al., 2022). Mass concentrations of $PM_{2.5}$, NO_2 and O_3 at MS site were directly quantified by E-BAM (Met One Instruments, USA) and NOx and O_3 Analyzer (Thermo, Model 42i, USA; Thermo, Model 49i, USA), respectively. At MF site, the data of above species apart from $PM_{2.5}$ monitored by another E-BAM were downloaded from the Weinan Ecological Environment Bureau (http://sthjj.weinan.gov.cn/, last access: 8 July 2021). Meteorological parameters of both sampling sites were downloaded from the Shaanxi Meteorological Bureau website (http://sn.cma.gov.cn/, last access: 8 July 2021).

2.2 Chemical Analysis

The organic carbon (OC) and element carbon (EC) of $PM_{2.5}$ filter samples were quantified by a DRI model 2001 thermal–optical carbon analyzer following the IMPROVE-A temperature protocol (Chow et al., 2007). Water-soluble organic carbon (WSOC) and water-soluble total nitrogen (WSTN) of $PM_{2.5}$ were extracted using Milli-Q pure water (18.2 MΩ) and determined using a total organic carbon (TOC) analyzer (Model TOC-L CPH, Shimadzu, Japan). Water-soluble organic nitrogen (WSON) is calculated by deducting the water-soluble inorganic nitrogen (WSIN) from WSTN (i.e., WSON=WSTN-WSIN). Molecular compositions (e.g.,

nitrophenols, PAHs and other organic tracers) in the $PM_{2.5}$ filter samples were quantified by a gas chromatography (HP 7890A, Agilent Co., USA) coupled with mass spectroscopy detector (GC/MS) (HP 5975, Agilent Co., USA) after the sample extraction and derivatization. Th details of the extraction and derivatization can be found elsewhere (Li et al., 2023; Li et al., 2020; Wang et al., 2006). Briefly, one-fourth of the filter sample was extracted with a mixture of methanol and dichloromethane (2:1, v/v). Then the extracts were derivatized with N,O-bis-(trimethylsilyl) trifluoroacetamide (BSTFA).

The stable nitrogen isotope compositions of NH_4^+ ($\delta^{15}N\text{-}NH_4^+$) were determined by the isotopic analysis of nitrous oxide (N_2O) derived from chemical conversion of NH_4^+, and finally quantified by a Precon-GasBench-IRMS system. This is a reliable method for nitrogen isotope analysis of the sample with low NH_4^+ concentration, of which precision can be up to 0.2‰. More details upon the analytical artifact and quality control protocols can be found in our previous studies. Furthermore, only the daytime samples were analyzed for the $\delta^{15}N\text{-}NH_4^+$ here, and a merging pretreatment was applied for the daily samples to meet for the analysis requirements.

Additionally, a high-resolution time-of-flight aerosol mass spectrometer (Aerodyne Research Inc., Billerica, MA, USA) was employed to determine the chemical compositions of water-soluble organic matter (WSOM) in $PM_{2.5}$, of which the method is similar to the report by Daellenbach et al. (2016). The offline analytical procedure has been reported previously, here we only give a brief description (Ge et al., 2017; Sun et al., 2011). One-eighth of the $PM_{2.5}$ filter samples was extracted with pure water. Then, the water-extracts were atomized using argon as carrier gas, dried by a diffusion drier, and ultimately quantified by the aerosol mass

spectrometer. Purified water was also treated in the same manner prior to each sample running, which was deemed as an analytical blank. As we mainly focused on the WSOM chemical composition, a deep post-processing was conducted for the V-mode data in this study using the Igor-based Aerosol Mass Spectrometer Analysis Toolkit. Element ratios of WSOM including oxygen-to-carbon (O/C), hydrogen-to-carbon (H/C), nitrogen-to-carbon (N/C) , and organic mass-to-organic carbon (OM/OC) ratios were determined according to the Improved Aiken (I-A) method (Canagaratna et al., 2015). The mass load of WSOM in ambient air can be accurately estimated using Eq.1, since the chemical species concentration in atomized aerosols depends on the flow rate of the carrier gas and extract concentration.

$$WSOM=WSOC\times OM/OC_{WSOM} \quad \text{Eq. 1}$$

Where WSOM is water-soluble organic matter (WSOM) in the atmosphere (μg m^{-3}), WSOC is water-soluble organic carbon (WSOC, μgCm^{-3}) in the atmosphere and measured by the TOC analyzer, and OM/OC_{WSOM} is the mass ratio of WSOM and OC determined by the aerosol mass spectrometer. To obtain reliable data, the ionization efficiencies of HR-AMS was calibrated with 300 nm (D_m) ammonium nitrate and ammonium sulfate particle following the standard protocols (Sun et al., 2020; Jayne et al., 2000); and the relative ionization efficiencies (RIEs) of 4.1 and 0.8 were used for ammonium and sulfate. While, the default RIEs were applied for organics, nitrate and chloride.

2.3 Optical Absorption of BrC

Measurement of UV−vis absorption spectra of water-soluble BrC in $PM_{2.5}$ was performed using a liquid waveguide capillary UV−vis spectrometer with a long effective path length (1 m). The extracted solution of BrC were prepared by a similar treatment to WSOC (Text S1), of

which absorption spectra were converted into the absorption coefficient at a given wavelength λ (abs_λ, M/m, eq S1). The mass absorption efficiency (MAE_λ, m^2/gC) corresponding to water-soluble BrC at a given wavelength λ can be calculated as follows:

$$MAE_\lambda = \frac{abs_\lambda}{M} \quad \text{Eq. 2}$$

Where M ($\mu gC/m^3$) is the mass concentration for water-soluble organic carbon (WSOC). Absorption Ångström exponent (AAE) indicates the spectral dependence of a species, which was quantified by a linear regression of log (abs_λ) versus log (λ) over a wavelength rang of 300-500 nm (Wu et al., 2020).

2.4 Positive matrix factorization (PMF) source apportionment

To quantitatively determine the fractional contribution of specific sources to BrC, a PMF receptor model (EPA PMF 5.0 version) coupled with a bootstrap technique was applied here, of which principle has been documented in previous studies (Brinkman et al., 2006; Paatero and Tapper, 1994). Briefly, WSOC, WSON, SO_4^{2-}, NH_4^+, Mg^{2+}, Ca^{2+}, $abs_{365\ nm}$ and organic tracers (BbF, Bghip and levo.) are the input variables in the present work, all of which are regarded as strong variable expect for Bghip with a low S/N ratio (0.6). Another input dataset is uncertainty matrix that is calculated according to the following equations (Eq.3). The uncertainties of each factor profile are also evaluated by a bootstrap analysis, of which result showed that reproducibility of each source factor was >80% (Table S1), indicating a well robustness. In our previous study on Mt. Hua (Wu et al., 2022), insignificant change in the corresponding emission sources was revealed during air mass lifting process. Thus, the daytime samples from both sites were added together as one data matrix. Considering Q values and interpretability, four factors were obtained as the optimal solution after numerous testes with three to seven factors, and the

input species matched well with simulated ones with significant correlations (R^2>0.88).

$$\text{uncertainty}=\begin{cases}\frac{5}{6}\times\text{MDL} & (\text{concentration}<\text{MDL})\\ \sqrt{(\text{error fraction}\times\text{concentration})^2+(0.5\times\text{MDL})^2} & (\text{concentration}>\text{MDL})\end{cases} \quad \text{Eq.3}$$

Where MDL is the method detection limit. And the error fraction is set to 5% for $PM_{2.5}$ (Gao et al., 2018); WSOC, WSON, SO_4^{2-}, NH_4^+, Mg^{2+}, Ca^{2+} are estimated to be 7 %, those of other species are 12%. To reduce the error, the sample with missing data for individual species would be excluded rather than replace by the mean value of whole campaign.

2.5 Random forest analysis for WSON

Random forest (RF), as a powerful tool, has been used widely in the regression and prediction problems upon atmospheric pollutions, even the data have complex nonlinear relationships and interactions (Hu et al., 2017; Vu et al., 2019). To reveal the key factors that may affect the WSON formation during the air mass lifting process, a RF regression model was applied for the daytime samples at MF and MS sites, respectively. And the potential factors, including pH, ALWC, T, RH, NH_4^+, NH_3(aq), NO_2, nitrophenols, O_3 and organic matter (OM), herein were regarded as the predictors for WSON. In the RF model design, about 70% of these original data were randomly divided into the training dataset to construct the RF model, and the rest was deemed as the testing data for testing the model performance. There are two important parameters being constantly optimized in the model construction process, including the number of trees grown (n_{tree}) and number of variables split at each node (n_{mtry}); After numerous tests, n_{tree} and n_{mtry} were set as 100 and 10 for MF data, and 128 and 9 for MS data, respectively, to achieve the best prediction accuracy. Furthermore, a 10-fold cross-validation technique was employed here to simultaneously tune model parameters and estimate model performance. And the statistical metrics including coefficient of determination (R^2), mean square error (MSE) or root-mean-

square error (RMSE) and mean absolute error (MAE), were established to evaluate prediction accuracy of the model. As shown in Table S2, the predicted data for the testing dataset has strong correlativity with observed ones, with small values for those error metrics; These results indicated a satisfactory performance of the RF model for explain the importance of these factors to daytime WSON formation.

3. Results and Discussion

3.1 Enhanced Light Absorption of BrC in the Mountainous Atmosphere

Figure 1 shows the temporal variations in light absorption (abs_{365nm}) and concentrations of fine particulate WSOC simultaneously observed at the mountain foot (MF) and mountainside (MS) sites. The variation patterns of water-soluble BrC (i.e., $abs_{365\ nm}$) at both sites were closed followed by WSOC (R^2>0.70, Figure 1 and Figure S2); this indicated that BrC is an important part of WSOC, of which light absorption of BrC markedly increased with a decrease in light wavelengths. As summarized in Table 1, the averaged $abs_{365\ nm}$ of BrC was 2.1±1.4 M m^{-1} at MS, approximately corresponding to 40% of that (5.1±2.4 M m^{-1}) at MF. The light-absorbance level of BrC at the high altitude MS site is in the same range as those reported from Chinese megacities such as Beijing (Cheng et al., 2016) and Xi'an (Wu et al., 2020), indicating a strong light-absorption of BrC in the upper boundary layer over Guanzhong Basin, inland China. Absorption Ångström exponent (AAE) at MS is 5.7±1.3 (Table 1), slightly lower than that at the ground MF site (6.0±0.5). Such a difference in AAE ($p<0.05$) is most likely related to the difference in chemical composition of the chromophores between the two sites with different altitudes. The averaged mass absorption efficiency (MAE) at MS ($MAE_{365\ nm}$, 0.67±0.2 $m^2\ g^{-1}$) was almost equal to that at MF (0.69±0.2 $m^2\ g^{-1}$) but 30-40% higher than those observed in

Chinese megacities such as Beijing (Du et al., 2014) and Nanjing (Chen et al., 2018) (~0.5 m^2 g^{-1}, in summertime), further demonstrating a strong light-absorption nature of BrC in the upper boundary layer of Guanzhong Basin, inland China.

Figure 2 shows the diurnal variations of $abs_{365\ nm}$ and $MAE_{365\ nm}$ at both sites during the campaign. At MF site a morning peak of $abs_{365\ nm}$ driven by enhanced traffic emissions occurred at 8:00~12:00 (local time, thereinafter), and then gradually decreased and reached a minimum at 12:00~16:00 with the lowest MAE at 365 nm wavelength ($MAE_{365\ nm}$, 0.57±0.14 m^2 g^{-1} (Figures 2a and 2b). Such a ground surface decease in light absorption of BrC at early afternoon can be attributed to the daytime boundary layer growth and photobleaching. This can be verified by the oxidation state of carbon (OSc) measured by the aerosol mass spectrometer, of which higher value is indicative of a deeper degree of atmospheric oxidation (Li et al., 2019a). As seen in Figure 3a, $abs_{365\ nm}$ negatively correlated with OSc, which is consistent with those reported by previous laboratory experiments (Lee et al., 2014; Zhao et al., 2015; Sumlin et al., 2017) and suggests that atmospheric aging can significantly diminish the light-absorption of BrC. On the contrary, abs_{365nm} at MS site remarkably enhanced with the boundary layer growth and peaked at 12:00~16:00 (Figure 2a), despite the fact that the aerosol was further oxidized during the upward transport as indicated by the a higher OSc value at MS site (Figure 3b); The OSc variation among both sites coincided with that of BaP/BeP being a known proxy of whether aerosols are freshly emitted (> 1) or aged (< 1) (Figure S3). Moreover, a moderate-increased MAE_{365nm} was also observed in this process (Figure 2b). As shown in Table 1, the light absorption of BrC at 365 nm relative to BC at 550 nm (abs_{365}-BrC/abs_{550}-BC) during the daytime at MS was 0.28±0.08, which is approximately 30% higher than that (0.22±0.08, Table

1) at MF. Our previous study at Mt. Hua found that changes in sources of primary organic aerosols in the air mass transported from MF to MS were insignificant (Wu et al., 2022), indicating that there was no additional emission of BrC during the air mass upward transport. Thus, the enhanced light-absorption of BrC relative to BC at MS is solely ascribed to a secondary formation of absorbing BrC (Figure 2c); and these secondary BrC were highly light-absorbing despite more aged atmosphere aloft, as verified by a strongly positive correlation between MAE_{365nm} and OSc values at MS site (Figure S4).

To further elucidate the above hypothesis, a PMF analysis was applied for the source apportionment of the daytime $abs_{365\ nm}$ at both sites. As seen in Figure S5, four types of BrC sources were identified. In brief, fossil fuel combustion and biomass burning influenced by local-related emissions were primary sources for the surface BrC, consistent with observations in other cities (Li et al., 2023; Wu et al., 2020; Wang et al., 2022a). However, BrC at MS site was produced dominantly from secondary formation, of which the contribution to the total BrC is 53% and about twice of that at MF (Figure 2d) further corroborating a substantial formation of BrC with relatively stronger light-absorptivity during the air mass lifting process. These secondarily formed BrC chromophores engender a more light-absorption of high-altitude BrC compared with that of BC (or EC, Figure 2c); Similar vertical profile of BrC in the upper troposphere (5~12 km) of the continental US was also observed by in-situ aircraft measurements (Zhang et al., 2017).

3.2 Secondary Formation of BrC in the Air Mass Lifting Process

Figure 4a illustrates the diurnal cycles of N:C ratio of the water-soluble organic matter in $PM_{2.5}$ measured by the high-resolution time-of-flight aerosol mass spectrometer. At the MF site

290 N:C ratio did not vary much with time and was even leveling off in the daytime, which
291 indicates that the compositions of light-absorbing chromophores are similar throughout the day.
292 Nonetheless, the diurnal pattern of N:C ratio at MS was analogous to that of $abs_{365\ nm}$ and
293 $MAE_{365\ nm}$ with a daily peak at 12:00~16:00 and a moderate positive correlation was also
294 observed between N:C ratio and $abs_{365\ nm}$ (R^2=0.38, P<0.01), suggesting that nitrogen-
295 containing organic compounds (NOCs) have significant contributions to the BrC light-
296 absorption in the upper boundary layer. Such a results is consistent with the laboratory
297 simulation, in which NOCs have been reported to contribute up to 60% of the absorbance of
298 secondary BrC over a wavelength rang of 300−400 nm (Lin et al., 2015). Moreover, the
299 daytime N:C ratios were 20% higher at MS (0.066±0.014) than those at MF (Figure 4a),
300 indicating that additional NOCs were produced in the air mas lifting process. In fact, numerous
301 N-containing organic fragments including C_xH_yN and $C_xH_yO_zN$ at the MS site were detected by
302 the aerosol mass spectrometer, accounting for ~13% of the total water-soluble OM; And
303 fractional contribution of above fragments at MS enhanced by approximately 10% compared to
304 that at MF site, even up to ~25% at the day with low $PM_{2.5}$ load (<75 μg/m^3) (Figure S6). This
305 suggested an enhanced formation of WSON during the air mass transport from the lower
306 mountain foot site to the upper mountainside site. Since WSON at MS moderately was
307 positively correlated with light absorption of BrC at λ=365nm (Figure S7, R^2=0.45, p<0.05),
308 the enhancement in BrC light-absorption at MS can largely be attributed to secondary
309 formation of NOCs during the air mass transport from the ground surface to the upper
310 boundary layer.
311 Light-absorbing NOCs including reduced nitrogen species (e.g., imidazoles and pyrazines)

and oxidized ones (e.g., nitroaromatics) can be generated via various types of gas- and particle-phase reactions, such as, NH_3-mediated carbonyl-to-imine reactions, nitration of aromatic compounds, and heterogeneous reactions of ·OH and NO_2^{-}· radicals with phenolic compounds (Moise et al., 2015; Laskin et al., 2015). The potential pathways and dominating factors for NOCs formation at MS site will be explored in the following sections.

3.3 Gas-Phase Formation of BrC in the Air Mass Lifting Process

Nitroaromatic compounds (NACs) are strong light-absorbing compounds and are ubiquitous in the atmosphere. In this study, a total of six NACs in the $PM_{2.5}$ samples were detected (Table S3), which exhibited a significant correlation with $abs_{365\ nm}$ at both sampling sites (Figure S2c and S2d), indicating an important impact of NACs on the aerosol light-absorption. As seen in Figure 5a, both NACs concentration and NACs/OC ratio decreased gradually at MF, reaching the daily minimum at 12:00-16:00. Such an abatement in NACs was mainly attributed to the boundary layer expansion and an enhanced photooxidation (Figure 3). Furthermore, the daytime NACs at MF well correlated with (BbF+levoglucosan) being known as tracers for combustion emissions (R^2>0.76, Figure 5c), but not correlated with gaseous NO_2 (Figure 5e), suggesting that most of NACs at the ground surface site were directly emitted from combustion sources. This can be further verified by a strong positive correlation of NACs and CO prevailing in combustion exhausts (Figure S8). As partial NACs at the MF site can be transported aloft by anabatic valley winds, thus a moderate correlation (R^2=0.49, Figure 5d) between NACs and (BbF+levoglucosan) was observed at MS site. However, a moderate correlation between NO_2 and NACs (R^2=0.57, $p<0.01$, Figure 5f) observed at MS suggests a non-negligible formation of secondary NACs under the transport process. As revealed by

previous studies, the NO_3·/·OH-oxidation of phenolic volatile organic in the presence of NOx can form numerous NACs that followed by partitioning to the condensed phase (Wang and Li, 2021; Li et al., 2021a; Finewax et al., 2018); and the photolysis of nitrite in aerosol aqueous phase can also lead to the nitration of phenol/catechol to generated NACs (Vione et al., 2005). But a poor relationship between NACs and aerosol liquid water content (ALWC; R^2=0.34, P>0.05) and particulate phenol (R^2<0.1), indicating a minor contribution of aqueous-phase formation to NACs aloft.

The preceding discussion provided reliable evidences that partial NACs could be formed by gas-phase reactions, but they only accounted for a very small fraction of OC (Figure 5a-b), suggesting that gas-phase formation is probably not the major formation pathway of secondary NOCs during the air mass vertical transport. Further evidence for this hypothesis was provided by a random forest (RF) analysis being used as a metric for the degree of correlation between these influencing factors (ALWC, pH, T, NO_2, NH_4^+, etc.) and WSON at both sampling sites (Figure 4b and Figure S9). As revealed by RF model results, nitrophenols and gaseous NO_2 were important influencing factors for the daytime WSON at MF site (Figure S9), of which importance was explained up to 35% but only~15% of that aloft (Figure 4b), confirming a less importance of the gas-phase reactions for the light-absorbing NOCs formation in the vertical transport process.

3.4 Aerosol Aqueous Formation of BrC in the Air Mass Lifting Process

As shown in Figure 4b, RF analysis showed that the variation in concentration of WSON in $PM_{2.5}$ at MS was largely affected by NH_4^+ (23.0%) and ALWC (17.3%). Given a relatively strong correlation between WSON and NH_4^+ (R^2=0.70, Figure 4c), we proposed that aqueous

phase reactions induced by ammonium is the major formation pathway for water-soluble NOCs at MS. For further demonstrating such a hypothesis, we analyzed nitrogen isotope composition ($\delta^{15}N\text{-}NH_4^+$) of ammonium in the $PM_{2.5}$ samples at both sites, of which the analytical details has been described in our previous study (Wu et al., 2022). As seen in Figure 4d, WSON showed a strong negative correlation with $\delta^{15}N\text{-}NH_4^+$, probably due to the irreversible reactions involving ammonia favored ^{15}N depletion in the particle form as revealed by Heaton et al. (1997). In contrast, WSON at MF presented a similar correlation with NH_4^+ as that at MS but did not correlate with $\delta^{15}N\text{-}NH_4^+$ (Figures S10 (a) and (b)).

Previous studies have demonstrated the importance of NH_4^+/NH_3 in the formation of light-absorbing imidazoles and N-heterocycles from the carbonyls (e.g., glyoxal (Gly) and methylglyoxal (mGly) generated from oxidation of VOCs) (Li et al., 2021b; Moise et al., 2015; Kampf et al., 2012; Liu et al., 2023). Figure S11 depicts a simple reaction pathway for above aqueous reactions, in which the chromophore products contain less amounts of O and H atoms. Such a phenomenon was found for the daytime NOCs at MS. As shown in Figure 6, the H/N and O/N ratios of BrC in $PM_{2.5}$ at MS exhibited a strongly negative correlation with N/C ratio, respectively (R^2=0.92 for H/N and R^2=0.84 for O/N). Considering the fact that Gly and mGly are abundant at the daytime atmosphere of Mt. Hua (Qi et al., 2023), the aqueous reactions of dicarbonyls with NH_4^+/NH_3 are probably the major pathway to yield NOCs during the vertical transport.

Above aqueous reactions could also occur at MF site as depicted in Figure S11, but it was insignificant compared to that at MS site, attributing the disparity in chemical compositions. Our previous study found that the ground surface MF aerosols were more acidic (pH=2.9) and

dominated by NH_4HSO_4, while the upper boundary layer MS aerosols were less acidic (pH=3.4) and dominated by abundant $(NH_4)_2SO_4$. Such differences in aerosol acidity and chemical compositions between two sites can favor the formation of NOCs at the MS site, as evident from a recent experimental observation by Li et al. (2021b), who found that NOCs yield on the $(NH_4)_2SO_4$ seeds exposing to Gly or mGly vapor was relatively higher than that on NH_4HSO_4 seeds. Also, they found that mGly has a larger uptake coefficient on $(NH_4)_2SO_4$ particles with a relatively higher NOCs yield compared to Gly, because mGly has a stronger interfacial attraction and thus has a more efficient nucleophilic addition involving the carbenium ions (Li et al., 2021b). Our previous study showed that the summertime atmosphere of Mt. Hua is dominated by biogenic VOCs and the concentration of fine particulate mGly is about five times that of Gly (Meng et al., 2014). Such a predominance of mGly over Gly and a less acidic aerosol aqueous aerosol phase at the MF site are favorable for light-absorbing NOCs formation on $(NH_4)_2SO_4$ particles, which can mainly be responsible for the enhanced light absorption of BrC at the mountainous site with the ratio of light absorption of BrC to BC higher in the upper boundary layer than that in the ground surface.

3.5 Atmospheric implications

Our work provides an evolution profile of BrC during air mass vertical transport, and highlights a secondary formation of BrC in this process, which can be responsible for the enhancement of BrC relative to BC in the upper boundary layer. As the longer lifetime of high-altitude BrC, they can disperse rapidly into a large area (Zhang et al., 2017), exerting significant influence on regional climate that is even comparable to BC in the upper tropical troposphere (Jo et al., 2016). Moreover, we also revealed a vital role of aqueous-phase

reactions for the secondary formation of BrC in the air mass lifting process, specifically the NH_4^+/NH_3-induced reactions (e.g., Maillard reaction) that can form NOCs with stronger light-absorptivity. As ammonia and carbonyls such as glyoxal and methylglyoxal are ubiquitous in the troposphere, thus our work suggests that the above formation mechanism on the light-absorbing NOC aerosols could extensively occur in the troposphere.

In the past decade, the haze pollution in China has changed from previous sulfate-dominated environment (SD) to the current nitrate-dominated environment (ND) due to the effective sulfur emission control, which would significantly enhance the aerosol ALWC since nitrate is more hygroscopic than sulfate at a given RH and aerosol loading. While, as indicated by our previous observational evidences (Lv et al., 2023), high ALWC load induced by abundant nitrate would efficiently promote more WSOC partitioning into the aerosol phase compared with that in SD ones, and thus may increase the BrC yield because WSOC contains numerous BrC precursors. With the increase in relative abundance of nitrate to sulfate, nitrate-enhanced gas-to-particle partitioning of WSOC will become highly efficient in China in the near future, meaning that the BrC formation will be more active hereafter. Additionally, the national VOCs and NH_3 emissions have remained at high levels, and even have shown a slight increasing trend. The abundant NH_3 can not only participates in the formation of BrC but also affects BrC optical properties by regulating the aerosol acidity. To further reveal the impact on the BrC, the NH_3 concentration and $MAE_{365\ nm}$ value of water-soluble BrC in different region of China were statistically explored on a national scale (Figure 7a). As depicted in Figure 7a, the spatial pattern of $MAE_{365\ nm}$ is closely coincident with NH_3 levels with a robust positive correlation (R^2=0.87). Such a spatial distribution pattern indicates that NH_3-rich conditions are

favorable for formation of BrC with strong light-absorptivity. China is one of the countries with strongest NH_3 emissions in the world due to huge demand for N-fertilizer (Van Damme et al., 2018), and thus atmospheric NH_3 in China is much higher than that in Europe and the United States. This is probably one of the factors causing the higher concentrations of BrC with stronger light-absorptivity in China compared with developed countries (Figure 7b).

4. Conclusion

Synchronous observations upon optical properties and chemical compositions of atmospheric BrC were conducted at MF and MS of Mt. Hua, and revealed that light-absorption of BrC aloft was only ~40% of that at surface owing to a dilution effect caused by planetary boundary layer upliftment. And the light-absorption of BrC relative to black carbon moderately enhanced in the lifting process of air mass from MF to MS coincide with the variation of the daytime MAE_{365nm} aloft, indicating a secondary formation of BrC; and these secondary BrC accounted for >50% of total at MS site. While, the surface BrC was mainly originated from direct combustion emission, with a 55% of fractional contribution to the total.

The N:C ratio of WSOM was measured by offline AMS, of which diurnal pattern was analogous to that of $abs_{365\ nm}$ and $MAE_{365\ nm}$ aloft, substantiating a considerable contribution of nitrogen-containing organic compounds (NOCs) to BrC light-absorption. And daytime N:C ratio site was approximately 15% higher at MS than that at MF, mainly due to a significant formation of secondary NOCs produced by NH_4^+/NH_3-induced reactions (e.g., Maillard reaction). Moreover, a robust positive relationship between $MAE_{365\ nm}$ and NH_3 load was statistically explored in nationwide, strongly manifested that abundant NH_3 maybe one of key factors for the high BrC load with strong light-absorptivity in China compared to that in

developed countries. Therefore, NH_3 emission control in China is indispensable for further alleviating haze and BrC pollutions in the country.

Data availability. The data used in this study are freely available at https://doi.org/10.5281/zenodo.10926469 (Wu, 2024). And Meteorological data and hourly $PM_{2.5}$, NO_2, O_3 concentrations can be obtained from https://doi.org/10.5281/zenodo.7413640 (Wu, 2022a).

Author contributions. G.W. designed research and contributed analytic tools. C.W., C.C. and J.L. collected the samples. C.W., X.L., K.Z. and G.W. conducted the sample analysis. C.W., S.Z. and G.W. performed the data interpretation. C.W. and G.W. wrote the paper. All authors contributed to the paper with useful scientific discussions.

Competing interests. The authors declare no competing interest.

Acknowledgements. This work was financially supported by the National Natural Science Foundation of China (No. 42130704, 42007202) and ECNU Happiness Flower program.

References

Bosch, C., Andersson, A., Kirillova, E. N., Budhavant, K., Tiwari, S., Praveen, P. S., Russell, L. M., Beres, N. D., Ramanathan, V., and Gustafsson, O.: Source-diagnostic dual-isotope composition and optical properties of water-soluble organic carbon and elemental carbon in the South Asian outflow intercepted over the Indian Ocean, J. Geophys. Res.-Atmos., 119, 11743-11759, 10.1002/2014jd022127, 2014.

Brinkman, G., Vance, G., Hannigan, M. P., and Milford, J. B.: Use of synthetic data to evaluate positive matrix factorization as a source apportionment tool for PM_{2.5} exposure data, Environ. Sci. Technol., 40, 1892-1901, 10.1021/es051712y, 2006.

Canagaratna, M. R., Jimenez, J. L., Kroll, J. H., Chen, Q., Kessler, S. H., Massoli, P., Hildebrandt Ruiz, L., Fortner, E., Williams, L. R., Wilson, K. R., Surratt, J. D., Donahue, N. M., Jayne, J. T., and Worsnop, D. R.: Elemental ratio measurements of organic compounds using aerosol mass spectrometry: characterization, improved calibration, and implications, Atmos. Chem. Phys., 15, 253-272, 10.5194/acp-15-253-2015, 2015.

Chakrabarty, R. K., Shetty, N. J., Thind, A. S., Beeler, P., Sumlin, B. J., Zhang, C., Liu, P., Idrobo, J. C., Adachi, K., Wagner, N. L., Schwarz, J. P., Ahern, A., Sedlacek, A. J., Lambe, A., Daube, C., Lyu, M., Liu, C., Herndon, S., Onasch, T. B., and Mishra, R.: Shortwave absorption by wildfire smoke dominated by dark brown carbon, Nat. Geosci., 16, 683-+, 10.1038/s41561-023-01237-9, 2023a.

Chakrabarty, R. K., Shetty, N. J., Thind, A. S., Beeler, P., Sumlin, B. J., Zhang, C. C., Liu, P., Idrobo, J. C., Adachi,

K., Wagner, N. L., Schwarz, J. P., Ahern, A., Sedlacek, A. J., Lambe, A., Daube, C., Lyu, M., Liu, C., Herndon, S., Onasch, T. B., and Mishra, R.: Shortwave absorption by wildfire smoke dominated by dark brown carbon, Nature Geoscience, 16, 10.1038/s41561-023-01237-9, 2023b.

Chen, Y., Ge, X., Chen, H., Xie, X., Chen, Y., Wang, J., Ye, Z., Bao, M., Zhang, Y., and Chen, M.: Seasonal light absorption properties of water-soluble brown carbon in atmospheric fine particles in Nanjing, China, Atmos. Environ., 187, 230-240, 10.1016/j.atmosenv.2018.06.002, 2018.

Cheng, Y., He, K.-b., Du, Z.-y., Engling, G., Liu, J.-m., Ma, Y.-l., Zheng, M., and Weber, R. J.: The characteristics of brown carbon aerosol during winter in Beijing, Atmos. Environ., 127, 355-364, 10.1016/j.atmosenv.2015.12.035, 2016.

Chow, J. C., Watson, J. G., Chen, L. W. A., Chang, M. C. O., Robinson, N. F., Trimble, D., and Kohl, S.: The IMPROVE-A temperature protocol for thermal/optical carbon analysis: maintaining consistency with a long-term database, Journal of the Air & Waste Management Association, 57, 1014-1023, 10.3155/1047-3289.57.9.1014, 2007.

Corbin, J. C., Czech, H., Massabo, D., de Mongeot, F. B., Jakobi, G., Liu, F., Lobo, P., Mennucci, C., Mensah, A. A., Orasche, J., Pieber, S. M., Prevot, A. S. H., Stengel, B., Tay, L. L., Zanatta, M., Zimmermann, R., El Haddad, I., and Gysel, M.: Infrared-absorbing carbonaceous tar can dominate light absorption by marine-engine exhaust, npj Clim. Atmos. Sci., 2, 10.1038/s41612-019-0069-5, 2019.

Daellenbach, K. R., Bozzetti, C., Krepelova, A. K., Canonaco, F., Wolf, R., Zotter, P., Fermo, P., Crippa, M., Slowik, J. G., Sosedova, Y., Zhang, Y., Huang, R. J., Poulain, L., Szidat, S., Baltensperger, U., El Haddad, I., and Prevot, A. S. H.: Characterization and source apportionment of organic aerosol using offline aerosol mass spectrometry, Atmospheric Measurement Techniques, 9, 23-39, 10.5194/amt-9-23-2016, 2016.

Druge, T., Nabat, P., Mallet, M., Michou, M., Remy, S., and Dubovik, O.: Modeling radiative and climatic effects of brown carbon aerosols with the ARPEGE-Climat global climate model, Atmos. Chem. Phys., 22, 12167-12205, 10.5194/acp-22-12167-2022, 2022.

Du, Z., He, K., Cheng, Y., Duan, F., Ma, Y., Liu, J., Zhang, X., Zheng, M., and Weber, R.: A yearlong study of water-soluble organic carbon in Beijing II: Light absorption properties, Atmospheric Environment, 89, 235-241, http://dx.doi.org/10.1016/j.atmosenv.2014.02.022, 2014.

Finewax, Z., de Gouw, J. A., and Ziemann, P. J.: Identification and Quantification of 4-Nitrocatechol Formed from OH and NO₃ Radical-Initiated Reactions of Catechol in Air in the Presence of NO_x: Implications for Secondary Organic Aerosol Formation from Biomass Burning, Environ. Sci. Technol., 52, 1981-1989, 10.1021/acs.est.7b05864, 2018.

Gao, J., Wang, K., Wang, Y., Liu, S., Zhu, C., Hao, J., Liu, H., Hua, S., and Tian, H.: Temporal-spatial characteristics and source apportionment of PM_{2.5} as well as its associated chemical species in the Beijing-Tianjin-Hebei region of China, Environ. Pollut., 233, 714-724, 10.1016/j.envpol.2017.10.123, 2018.

Ge, X., Li, L., Chen, Y., Chen, H., Wu, D., Wang, J., Xie, X., Ge, S., Ye, Z., Xu, J., and Chen, M.: Aerosol characteristics and sources in Yangzhou, China resolved by offline aerosol mass spectrometry and other techniques, Environ. Pollut., 225, 74-85, 10.1016/j.envpol.2017.03.044, 2017.

Gelencser, A., Hoffer, A., Kiss, G., Tombacz, E., Kurdi, R., and Bencze, L.: In-situ formation of light-absorbing organic matter in cloud water, Journal of Atmospheric Chemistry, 45, 25-33, 10.1023/a:1024060428172, 2003.

Gilardoni, S., Massoli, P., Paglione, M., Giulianelli, L., Carbone, C., Rinaldi, M., Decesari, S., Sandrini, S., Costabile, F., Gobbi, G. P., Pietrogrande, M. C., Visentin, M., Scotto, F., Fuzzi, S., and Facchini, M. C.: Direct observation of aqueous secondary organic aerosol from biomass-burning emissions, Proceedings of the National Academy of Sciences of the United States of America, 113, 10013-10018, 10.1073/pnas.1602212113, 2016.

Gligorovski, S., Strekowski, R., Barbati, S., and Vione, D.: Environmental Implications of Hydroxyl Radicals (•OH),

519 Chem. Rev., 115, 13051-13092, 10.1021/cr500310b, 2015.
520 Hammer, M. S., Martin, R. V., van Donkelaar, A., Buchard, V., Torres, O., Ridley, D. A., and Spurr, R. J. D.:
521 Interpreting the ultraviolet aerosol index observed with the OMI satellite instrument to understand absorption
522 by organic aerosols: implications for atmospheric oxidation and direct radiative effects, Atmos. Chem. Phys.,
523 16, 2507-2523, 10.5194/acp-16-2507-2016, 2016.
524 Heaton, T. H. E., Spiro, B., Madeline, S., and Robertson, C.: Potential canopy influences on the isotopic composition
525 of nitrogen and sulphur in atmospheric deposition, Oecologia, 109, 600-607, 10.1007/s004420050122, 1997.
526 Hodnebrog, O., Myhre, G., and Samset, B. H.: How shorter black carbon lifetime alters its climate effect, Nature
527 Communications, 5, 10.1038/ncomms6065, 2014.
528 Hsu, H.-I., Lin, M.-Y., Chen, Y.-C., Chen, W.-Y., Yoon, C., Chen, M.-R., and Tsai, P.-J.: An Integrated Approach to
529 Assess Exposure and Health-Risk from Polycyclic Aromatic Hydrocarbons (PAHs) in a Fastener
530 Manufacturing Industry, International Journal of Environmental Research and Public Health, 11, 9578-9594,
531 10.3390/ijerph110909578, 2014.
532 Hu, X., Belle, J. H., Meng, X., Wildani, A., Waller, L. A., Strickland, M. J., and Liu, Y.: Estimating
533 PM_{2.5} Concentrations in the Conterminous United States Using the Random Forest Approach,
534 Environ. Sci. Technol., 51, 6936-6944, 10.1021/acs.est.7b01210, 2017.
535 Huang, R.-J., Yang, L., Cao, J., Chen, Y., Chen, Q., Li, Y., Duan, J., Zhu, C., Dai, W., Wang, K., Lin, C., Ni, H.,
536 Corbin, J. C., Wu, Y., Zhang, R., Tie, X., Hoffmann, T., O'Dowd, C., and Dusek, U.: Brown Carbon Aerosol in
537 Urban Xi'an, Northwest China: The Composition and Light Absorption Properties, Environ. Sci. Technol., 52,
538 6825-6833, 10.1021/acs.est.8b02386, 2018.
539 Jayne, J. T., Leard, D. C., Zhang, X. F., Davidovits, P., Smith, K. A., Kolb, C. E., and Worsnop, D. R.: Development
540 of an aerosol mass spectrometer for size and composition analysis of submicron particles, Aerosol Sci. Technol.,
541 33, 49-70, 10.1080/027868200410840, 2000.
542 Jo, D. S., Park, R. J., Lee, S., Kim, S.-W., and Zhang, X.: A global simulation of brown carbon: implications for
543 photochemistry and direct radiative effect, Atmos. Chem. Phys., 16, 3413-3432, 10.5194/acp-16-3413-2016,
544 2016.
545 Kampf, C. J., Jakob, R., and Hoffmann, T.: Identification and characterization of aging products in the
546 glyoxal/ammonium sulfate system - implications for light-absorbing material in atmospheric aerosols, Atmos.
547 Chem. Phys., 12, 6323-6333, 10.5194/acp-12-6323-2012, 2012.
548 Laskin, A., Laskin, J., and Nizkorodov, S. A.: Chemistry of Atmospheric Brown Carbon, Chem. Rev., 115, 4335-
549 4382, 10.1021/cr5006167, 2015.
550 Laskin, J., Laskin, A., Nizkorodov, S. A., Roach, P., Eckert, P., Gilles, M. K., Wang, B., Lee, H. J., and Hu, Q.:
551 Molecular Selectivity of Brown Carbon Chromophores, Environ. Sci. Technol., 48, 12047-12055,
552 10.1021/es503432r, 2014.
553 Lee, H. J., Aiona, P. K., Laskin, A., Laskin, J., and Nizkorodov, S. A.: Effect of Solar Radiation on the Optical
554 Properties and Molecular Composition of Laboratory Proxies of Atmospheric Brown Carbon, Environ. Sci.
555 Technol., 48, 10217-10226, 10.1021/es502515r, 2014.
556 Li, D., Wu, C., Zhang, S., Lei, Y., Lv, S., Du, W., Liu, S., Zhang, F., Liu, X., Liu, L., Meng, J., Wang, Y., Gao, J.,
557 and Wang, G.: Significant coal combustion contribution to water-soluble brown carbon during winter in Xingtai,
558 China: Optical properties and sources, J. Environ. Sci., 124, 892-900, 10.1016/j.jes.2022.02.026, 2023.
559 Li, J., Zhang, Q., Wang, G., Li, J., Wu, C., Liu, L., Wang, J., Jiang, W., Li, L., Ho, K. F., and Cao, J.: Optical
560 properties and molecular compositions of water-soluble and water-insoluble brown carbon (BrC) aerosols in
561 northwest China, Atmos. Chem. Phys., 20, 4889-4904, 10.5194/acp-20-4889-2020, 2020.
562 Li, L. J., Ho, S. S. H., Feng, B., Xu, H., Wang, T., Wu, R., Huang, W., Qu, L., Wang, Q., and Cao, J.: Characterization

of particulate-bound polycyclic aromatic compounds (PACs) and their oxidations in heavy polluted atmosphere: A case study in urban Beijing, China during haze events, Sci. Total Environ., 660, 1392-1402, 10.1016/j.scitotenv.2019.01.078, 2019a.

Li, X., Hu, M., Wang, Y., Xu, N., Fan, H., Zong, T., Wu, Z., Guo, S., Zhu, W., Chen, S., Dong, H., Zeng, L., Yu, X., and Tang, X.: Links between the optical properties and chemical compositions of brown carbon chromophores in different environments: Contributions and formation of functionalized aromatic compounds, Sci. Total Environ., 786, 10.1016/j.scitotenv.2021.147418, 2021a.

Li, Y., Ji, Y., Zhao, J., Wang, Y., Shi, Q., Peng, J., Wang, Y., Wang, C., Zhang, F., Wang, Y., Seinfeld, J. H., and Zhang, R.: Unexpected Oligomerization of Small alpha-Dicarbonyls for Secondary Organic Aerosol and Brown Carbon Formation, Environ. Sci. Technol., 55, 4430-4439, 10.1021/acs.est.0c08066, 2021b.

Li, Z., Nizkorodov, S. A., Chen, H., Lu, X., Yang, X., and Chen, J.: Nitrogen-containing secondary organic aerosol formation by acrolein reaction with ammonia/ammonium, Atmos. Chem. Phys., 19, 1343-1356, 10.5194/acp-19-1343-2019, 2019b.

Lin, G., Penner, J. E., Flanner, M. G., Sillman, S., Xu, L., and Zhou, C.: Radiative forcing of organic aerosol in the atmosphere and on snow: Effects of SOA and brown carbon, J. Geophys. Res.-Atmos., 119, 7453-7476, 10.1002/2013jd021186, 2014.

Lin, P., Liu, J., Shilling, J. E., Kathmann, S. M., Laskin, J., and Laskin, A.: Molecular characterization of brown carbon (BrC) chromophores in secondary organic aerosol generated from photo-oxidation of toluene, Physical Chemistry Chemical Physics, 17, 23312-23325, 10.1039/c5cp02563j, 2015.

Liu, D., He, C., Schwarz, J. P., and Wang, X.: Lifecycle of light-absorbing carbonaceous aerosols in the atmosphere, npj Clim. Atmos. Sci., 3, 40, 10.1038/s41612-020-00145-8, 2020a.

Liu, S., Huang, D., Wang, Y., Zhang, S., Liu, X., Wu, C., Du, W., and Wang, G.: Synergetic effects of NH3 and NOx on the production and optical absorption of secondary organic aerosol formation from toluene photooxidation, Atmos. Chem. Phys., 21, 17759-17773, 10.5194/acp-21-17759-2021, 2021.

Liu, S., Aiken, A. C., Gorkowski, K., Dubey, M. K., Cappa, C. D., Williams, L. R., Herndon, S. C., Massoli, P., Fortner, E. C., Chhabra, P. S., Brooks, W. A., Onasch, T. B., Jayne, J. T., Worsnop, D. R., China, S., Sharma, N., Mazzoleni, C., Xu, L., Ng, N. L., Liu, D., Allan, J. D., Lee, J. D., Fleming, Z. L., Mohr, C., Zotter, P., Szidat, S., and Prevot, A. S. H.: Enhanced light absorption by mixed source black and brown carbon particles in UK winter, Nature Communications, 6, 10.1038/ncomms9435, 2015.

Liu, X., Wang, H., Wang, F., Lv, S., Wu, C., Zhao, Y., Zhang, S., Liu, S., Xu, X., Lei, Y., and Wang, G.: Secondary Formation of Atmospheric Brown Carbon in China Haze: Implication for an Enhancing Role of Ammonia, Environ. Sci. Technol., 57, 11163-11172, 10.1021/acs.est.3c03948, 2023.

Liu, Y., Wang, T., Fang, X., Deng, Y., Cheng, H., Bacha, A.-U.-R., Nabi, I., and Zhang, L.: Brown carbon: An underlying driving force for rapid atmospheric sulfate formation and haze event, Sci. Total Environ., 734, 139415, 10.1016/j.scitotenv.2020.139415, 2020b.

Lu, J. W., Flores, J. M., Lavi, A., Abo-Riziq, A., and Rudich, Y.: Changes in the optical properties of benzo a pyrene-coated aerosols upon heterogeneous reactions with NO2 and NO3, Physical Chemistry Chemical Physics, 13, 6484-6492, 10.1039/c0cp02114h, 2011.

Lv, S., Wu, C., Wang, F., Liu, X., Zhang, S., Chen, Y., Zhang, F., Yang, Y., Wang, H., Huang, C., Fu, Q., Duan, Y., and Wang, G.: Nitrate-Enhanced Gas-to-Particle-Phase Partitioning of Water- Soluble Organic Compounds in Chinese Urban Atmosphere: Implications for Secondary Organic Aerosol Formation, Environmental Science & Technology Letters, 10, 14-20, 10.1021/acs.estlett.2c00894, 2023.

Meng, J., Wang, G., Li, J., Cheng, C., Ren, Y., Huang, Y., Cheng, Y., Cao, J., and Zhang, T.: Seasonal characteristics of oxalic acid and related SOA in the free troposphere of Mt. Hua, central China: Implications for sources and

formation mechanisms, Sci. Total Environ., 493, 1088-1097, 10.1016/j.scitotenv.2014.04.086, 2014.
Moise, T., Flores, J. M., and Rudich, Y.: Optical Properties of Secondary Organic Aerosols and Their Changes by Chemical Processes, Chem. Rev., 115, 4400-4439, 10.1021/cr5005259, 2015.
Nazarenko, L., Rind, D., Tsigaridis, K., Del Genio, A. D., Kelley, M., and Tausnev, N.: Interactive nature of climate change and aerosol forcing, J. Geophys. Res.-Atmos., 122, 3457-3480, 10.1002/2016jd025809, 2017.
Paatero, P. and Tapper, U.: Positive matrix factorization: A non-negative factor model with optimal utilization of error estimates of data values, Environmetrics, 5, 111-126, https://doi.org/10.1002/env.3170050203, 1994.
Qi, W. N., Zhang, Y. F., Shen, M. X., Li, L., Dai, W. T., Chen, Y. K., Liu, Y. L., Guo, X., Cao, Y., Wang, X., Jiang, Y. K., and Li, J. J.: Comparison of Gas-Particle Partitioning of Glyoxal and Methylglyoxal in the Summertime Atmosphere at the Foot and Top of Mount Hua, Molecules, 28, 10.3390/molecules28135276, 2023.
Qian, Y., Yasunari, T. J., Doherty, S. J., Flanner, M. G., Lau, W. K. M., Ming, J., Wang, H., Wang, M., Warren, S. G., and Zhang, R.: Light-absorbing Particles in Snow and Ice: Measurement and Modeling of Climatic and Hydrological impact, Adv. Atmos. Sci., 32, 64-91, 10.1007/s00376-014-0010-0, 2015.
Saleh, R., Marks, M., Heo, J., Adams, P. J., Donahue, N. M., and Robinson, A. L.: Contribution of brown carbon and lensing to the direct radiative effect of carbonaceous aerosols from biomass and biofuel burning emissions, J. Geophys. Res.-Atmos., 120, 10285-10296, 10.1002/2015jd023697, 2015.
Schnitzler, E. G., Gerrebos, N. G. A., Carter, T. S., Huang, Y., Healdc, C. L., Bertram, A. K., and Abbatt, J. P. D.: Rate of atmospheric brown carbon whitening governed by environmental conditions, Proceedings of the National Academy of Sciences of the United States of America, 119, 10.1073/pnas.2205610119, 2022.
Sumlin, B. J., Pandey, A., Walker, M. J., Pattison, R. S., Williams, B. J., and Chakrabarty, R. K.: Atmospheric Photooxidation Diminishes Light Absorption by Primary Brown Carbon Aerosol from Biomass Burning, Environmental Science & Technology Letters, 4, 540-545, 10.1021/acs.estlett.7b00393, 2017.
Sun, Y., Zhang, Q., Zheng, M., Ding, X., Edgerton, E. S., and Wang, X.: Characterization and Source Apportionment of Water-Soluble Organic Matter in Atmospheric Fine Particles (PM2.5) with High-Resolution Aerosol Mass Spectrometry and GC-MS, Environ. Sci. Technol., 45, 4854-4861, 10.1021/es200162h, 2011.
Sun, Y., Lei, L., Zhou, W., Chen, C., He, Y., Sun, J., Li, Z., Xu, W., Wang, Q., Ji, D., Fu, P., Wang, Z., and Worsnop, D. R.: A chemical cocktail during the COVID-19 outbreak in Beijing, China: Insights from six-year aerosol particle composition measurements during the Chinese New Year holiday, Sci. Total Environ., 742, 10.1016/j.scitotenv.2020.140739, 2020.
Van Damme, M., Clarisse, L., Whitburn, S., Hadji-Lazaro, J., Hurtmans, D., Clerbaux, C., and Coheur, P.-F.: Industrial and agricultural ammonia point sources exposed, Nat., 564, 99-103, 10.1038/s41586-018-0747-1, 2018.
Vione, D., Maurino, V., Minero, C., and Pelizzetti, E.: Aqueous atmospheric chemistry: Formation of 2,4-dinitrophenol upon nitration of 2-nitrophenol and 4-nitrophenol in solution, Environ. Sci. Technol., 39, 7921-7931, 10.1021/es050824m, 2005.
Vu, T. V., Shi, Z., Cheng, J., Zhang, Q., He, K., Wang, S., and Harrison, R. M.: Assessing the impact of clean air action on air quality trends in Beijing using a machine learning technique, Atmos. Chem. Phys., 19, 11303-11314, 10.5194/acp-19-11303-2019, 2019.
Wang, D., Shen, Z., Zhang, Q., Lei, Y., Zhang, T., Huang, S., Sun, J., Xu, H., and Cao, J.: Winter brown carbon over six of China's megacities: light absorption, molecularcharacterization, and improved source apportionment revealed by multilayerperceptron neural network, Atmos. Chem. Phys., 22, 14893-14904, 10.5194/acp-22-14893-2022, 2022a.
Wang, G., Li, J., Cheng, C., Hu, S., Xie, M., Gao, S., Zhou, B., Dai, W., Cao, J., and An, Z.: Observation of atmospheric aerosols at Mt. Hua and Mt. Tai in central and east China during spring 2009-Part 1: EC, OC and

inorganic ions, Atmos. Chem. Phys., 11, 4221-4235, 10.5194/acp-11-4221-2011, 2011.
Wang, G. H., Kawamura, K., Lee, S., Ho, K. F., and Cao, J. J.: Molecular, seasonal, and spatial distributions of organic aerosols from fourteen Chinese cities, Environmental Science & Technology, 40, 4619-4625, 10.1021/es060291x, 2006.
Wang, G. H., Zhang, R. Y., Gomez, M. E., Yang, L. X., Zamora, M. L., Hu, M., Lin, Y., Peng, J. F., Guo, S., Meng, J. J., Li, J. J., Cheng, C. L., Hu, T. F., Ren, Y. Q., Wang, Y. S., Gao, J., Cao, J. J., An, Z. S., Zhou, W. J., Li, G. H., Wang, J. Y., Tian, P. F., Marrero-Ortiz, W., Secrest, J., Du, Z. F., Zheng, J., Shang, D. J., Zeng, L. M., Shao, M., Wang, W. G., Huang, Y., Wang, Y., Zhu, Y. J., Li, Y. X., Hu, J. X., Pan, B., Cai, L., Cheng, Y. T., Ji, Y. M., Zhang, F., Rosenfeld, D., Liss, P. S., Duce, R. A., Kolb, C. E., and Molina, M. J.: Persistent sulfate formation from London Fog to Chinese haze, Proceedings of the National Academy of Sciences of the United States of America, 113, 13630-13635, 10.1073/pnas.1616540113, 2016.
Wang, Q., Zhou, Y., Ma, N., Zhu, Y., Zhao, X., Zhu, S., Tao, J., Hong, J., Wu, W., Cheng, Y., and Su, H.: Review of Brown Carbon Aerosols in China: Pollution Level, Optical Properties, and Emissions, J. Geophys. Res.-Atmos., 127, 10.1029/2021jd035473, 2022b.
Wang, S. and Li, H.: NO3 center dot-Initiated Gas-Phase Formation of Nitrated Phenolic Compounds in Polluted Atmosphere, Environ. Sci. Technol., 55, 2899-2907, 10.1021/acs.est.0c08041, 2021.
Wu, C., Cao, C., Li, J., Lv, S., Li, J., Liu, X., Zhang, S., Liu, S., Zhang, F., Meng, J., and Wang, G.: Different physicochemical behaviors of nitrate and ammonium duringtransport: a case study on Mt. Hua, China, Atmos. Chem. Phys., 22, 15621-15635, 10.5194/acp-22-15621-2022, 2022.
Wu, C., Wang, G., Li, J., Li, J., Cao, C., Ge, S., Xie, Y., Chen, J., Li, X., Xue, G., Wang, X., Zhao, Z., and Cao, F.: The characteristics of atmospheric brown carbon in Xi'an, inland China: sources, size distributions and optical properties, Atmos. Chem. Phys., 20, 2017-2030, 10.5194/acp-20-2017-2020, 2020.
Wu, C., Observation of Brown carbon and its optical properties on Mt. Hua, Zenodo [data set], https://doi.org/10.5281/zenodo.10926470, 2024.
Wu, C., Synchronous observation of aerosol at Mt. Hua, Version 1, Zenodo [data set], https://doi.org/10.5281/zenodo.7413640, 2022a.
Yan, C., Zheng, M., Bosch, C., Andersson, A., Desyaterik, Y., Sullivan, A. P., Collett, J. L., Zhao, B., Wang, S., He, K., and Gustafsson, O.: Important fossil source contribution to brown carbon in Beijing during winter, Sci. Rep., 7, 10.1038/srep43182, 2017.
Yan, J., Wang, X., Gong, P., Wang, C., and Cong, Z.: Review of brown carbon aerosols: Recent progress and perspectives, Sci. Total Environ., 634, 1475-1485, 10.1016/j.scitotenv.2018.04.083, 2018.
Zhang, A., Wang, Y., Zhang, Y., Weber, R. J., Song, Y., Ke, Z., and Zou, Y.: Modeling the global radiative effect of brown carbon: a potentially larger heating source in the tropical free troposphere than black carbon, Atmos. Chem. Phys., 20, 1901-1920, 10.5194/acp-20-1901-2020, 2020.
Zhang, Y., Forrister, H., Liu, J., Dibb, J., Anderson, B., Schwarz, J. P., Perring, A. E., Jimenez, J. L., Campuzano-Jost, P., Wang, Y., Nenes, A., and Weber, R. J.: Top-of-atmosphere radiative forcing affected by brown carbon in the upper troposphere, Nat. Geosci., 10, 486-489, 10.1038/ngeo2960, 2017.
Zhao, R., Lee, A. K. Y., Huang, L., Li, X., Yang, F., and Abbatt, J. P. D.: Photochemical processing of aqueous atmospheric brown carbon, Atmos. Chem. Phys., 15, 6087-6100, 10.5194/acp-15-6087-2015, 2015.

691
692
693
694
695
696
697 **Table 1** Optical properties of BrC and mass concentrations organic carbon/nitrogen in $PM_{2.5}$ and
698 meteorological parameters at the two sampling sites.
699

	Mountain foot (MF)			Mountainside (MS)		
	Average	Daytime	Nighttime	Average	Daytime	Nighttime
(i) Optical properties of BrC and acidity of $PM_{2.5}$						
abs_{365} (M m^{-1})	5.1±2.4	5.0±2.5	5.2±2.2	2.1±1.4	2.6±1.3	1.6±1.3
MAE_{365} (m^2 g^{-1})	0.69±0.2	0.66±0.18	0.73±0.18	0.67±0.21	0.67±0.15	0.68±0.26
AAE	6.0±0.5	6.1±0.51	6.0±0.51	5.7±1.3	5.5±0.9	5.8±1.7
abs_{365}-BrC/abs_{550}-BC[a]	0.18±0.09	0.22±0.08	0.17±0.09	0.26±0.08	0.28±0.08	0.25±0.07
pH	2.9±2.0	2.3±1.6	3.6±2.1	3.4±2.2	3.5±2.2	3.3±2.2
(ii) Concentrations of carbonaceous $PM_{2.5}$ and aerosol liquid water content (ALWC)						
WSOC (μgC m^{-3})	7.3±2.5	7.6±2.8	7.0±2.1	3.2±2.1	4.0±2.1	2.4±1.7
WSON (μgN m^{-3})	2.3±1.6	2.5±1.7	2.0±1.4	1.2±0.9	1.5±1.1	0.8±0.7
OC (μgC m^{-3})	14.0±4.7	12.4±4.6	15.4±4.4	5.0±2.8	6.3±2.8	3.8±2.3
EC (μgC m^{-3})	4.3±2.0	3.1±1.0	5.4±1.9	1.1±0.7	1.3±0.7	0.8±0.4
Nitrophenols (ng m^{-3})	16±13	12±10	19±15	2.5±1.9	3.2±2.2	1.7±1.1
ALWC (μg m^{-3})	28±64	11±15	44±86	27±71	18±24	35±95
WSOC/OC	0.54±0.15	0.62±0.13	0.47±0.11	0.62±0.21	0.62±0.16	0.61±0.25
(iii) Meteorological parameters						
T (°C)	23±4.2	27±3.0	20±2.4	15±2.5	16±2.3	14±2.3
RH (%)	69±18	56±14	81±14	63±20	62±19	63±21
Wind speed (m s^{-1})	1.3±1.1	1.5±0.93	1.2±1.2	3.2±2.0	2.7±1.5	3.8±2.3
Visibility (km)	14±9.5	16±9.6	12±9.0	22±12.1	21±12	24±12.0

700 [a]The $abs_{550\text{-BC}}$ was calculated according to the mass absorption efficiency (MAE) of BC (black
701 carbon) reported by Bosch et al. (2014), and the light wavelengths for the abs_{365}-BrC and abs_{550}-
702 BC are 365 nm and 550 nm, respectively.
703

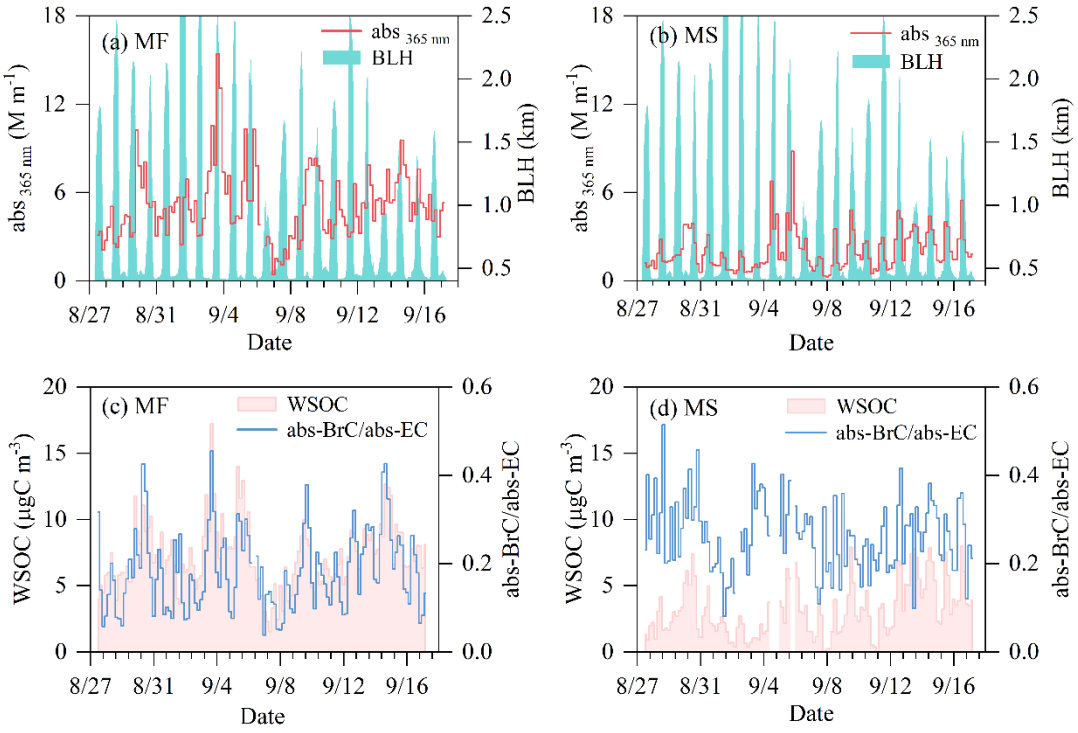

Figure 1. Temporal variations of light absorption of BrC in the ground surface (mountain foot site, MF) and the upper boundary layer (mountainside site, MS) atmospheres in inland China. (a, b) Abs_{365} and boundary layer height (BLH). (c, d) Concentration of WSOC and the ratio of light absorption of BrC at λ=365 nm to BC at λ= 550 nm.

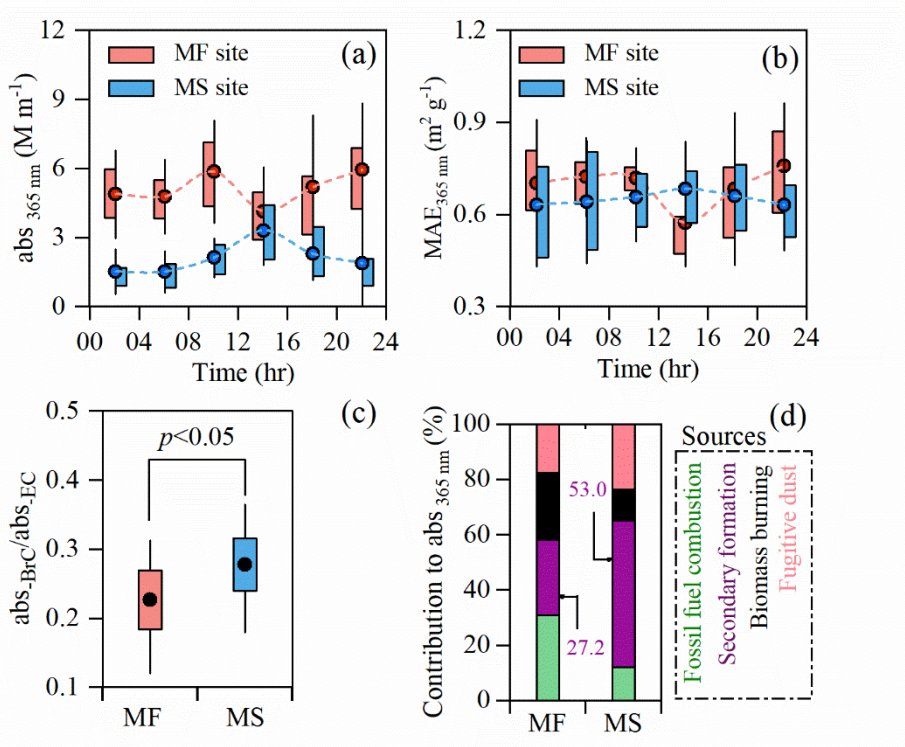

Figure 2. BrC formation in air mass lifting process. (a) and (b) Diurnal variations in abs_{365nm} and MAE at the mountain foot (MF) and mountainside (MS) sites. (c) Ratio of light absorption of BrC at λ=365 nm to that of BC (abs_{-BrC}/abs_{-BC}) at λ=550 nm in daytime at both sites (The abs_{-BC} at λ=550 nm was calculated according to mass absorption efficiency of EC reported by Bosch et al. (2014). (d) Source apportionment for the daytime BrC at the two sites. The whisker boxes show mean (dot), 25th–75th percentile ranges (box), and standard deviation values (whiskers).

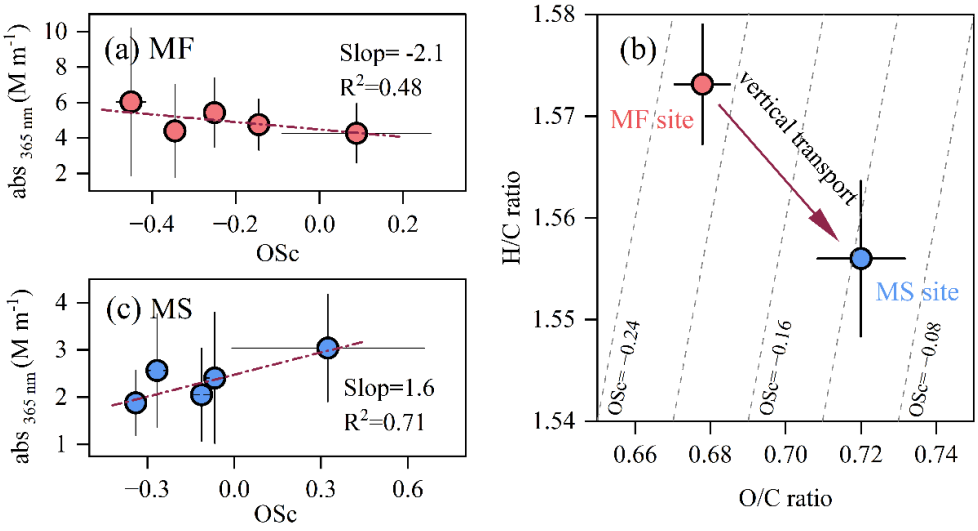

Figure 3. Evolution in chemical composition of daytime water-soluble BrC in the air mass transport from the mountain foot (MF site, red dots) to the mountainside (MS site, blue dots). (a) and (c) Light absorption (abs_{365}) of daytime water-soluble BrC as a function of their oxidation state (OSc=2O/C−H/C) at MF and MS sites, respectively. (b) The VK-triangle diagram of water-soluble BrC at the two sites.

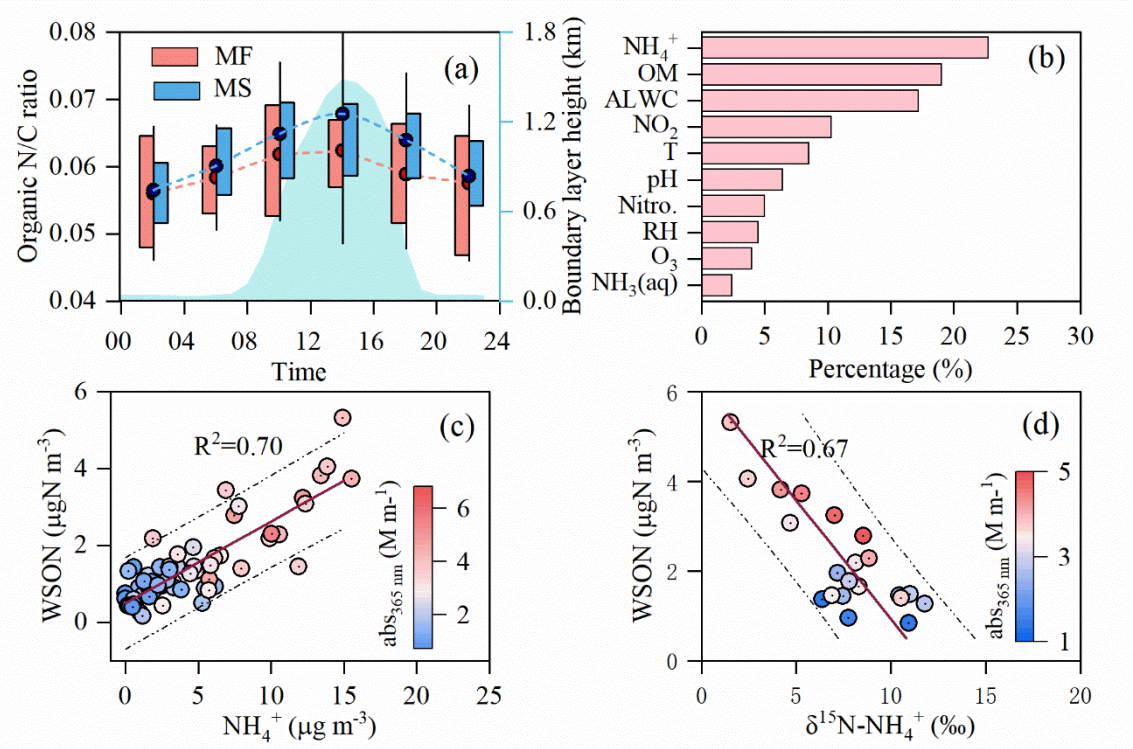

Figure 4. Formation of water-soluble organic nitrogen compounds (WSONs) in the air mass lifting process. (a) Diurnal variations in elemental ratio of N/C of fine particulate water-soluble organics at the mountain foot (MF) and mountainside (MS) sites, the whisker boxes show mean (dot), 25th–75th percentile ranges (box), and standard deviation values (whiskers). (b) Importance assessment for the key factors affecting the daytime WSON at MS site. (c) and (d) Linear fit regressions for WSONs with NH_4^+ and $\delta^{15}N\text{-}NH_4^+$ in the daytime $PM_{2.5}$ aerosols at MS site, respectively.

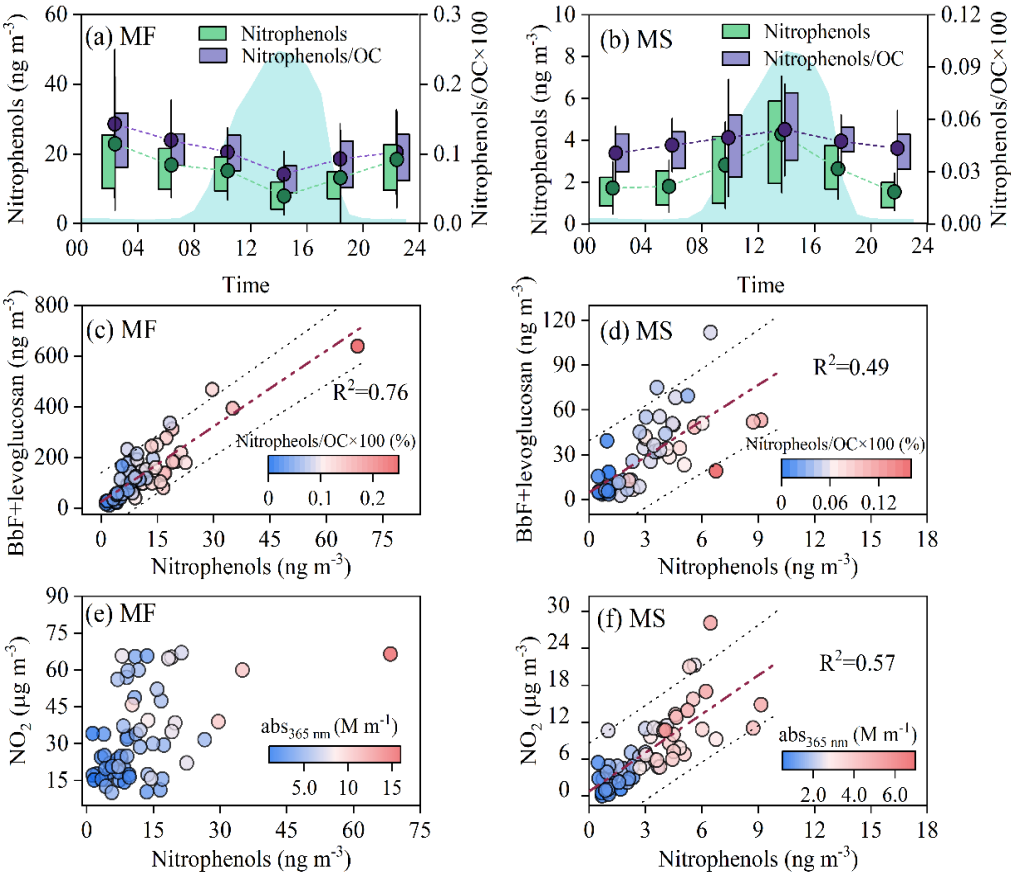

Figure 5. The source and secondary formation for nitrophenols at MF and MS sites. (a and b) Diurnal variations in nitrophenols and mass ratio of nitrophenols to OC (nitrophenols/OC); blue sky shade indicates diurnal variation of boundary layer height, and the whisker boxes show mean (dot), 25th–75th percentile ranges (box), and standard deviation values (whiskers). Linear fit regression for nitrophenols with BbF+levoglucosan (c and d) and NO_2 (e and f), respectively.

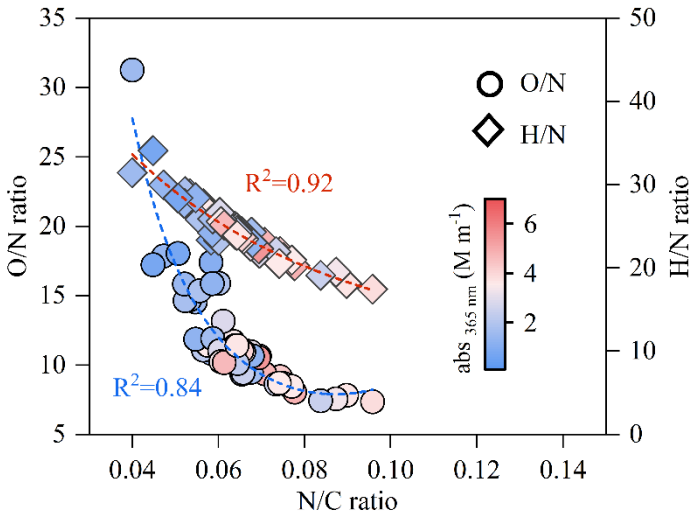

Figure 6. Elemental composition of daytime WSOC at MS site.

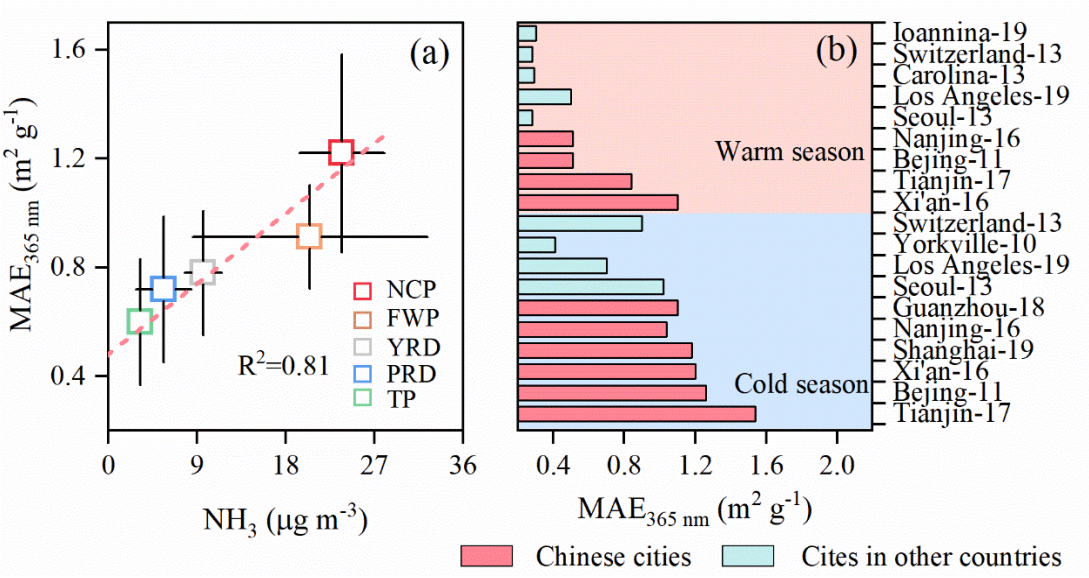

Figure 7. Impact of NH_3 on atmospheric BrC over China. (a) Linear correlation between NH_3 and MAE of BrC in different regions of China (NCP, north China Plain; FWP: Fenwei Plain; YRD, Yangtze River delta; PRD, Pearl River delta; TP: Tibetan Plain). (b) MAE_{365} of BrC in China and other countries (The details of datasets from literatures, including specific sites, time periods, and sources, etc., are given in Table S4 and S5).